Journal of Biomechanics 70 (2018) 157–165

Contents lists available at ScienceDirect

Journal of Biomechanics

journal homepage: www.elsevier.com/locate/jbiomech
www.JBiomech.com

A combined passive and active musculoskeletal model study to estimate L4-L5 load sharing

F. Azari [a], N. Arjmand [a,*], A. Shirazi-Adl [b], T. Rahimi-Moghaddam [a]

[a] Department of Mechanical Engineering, Sharif University of Technology, Tehran, Iran
[b] Division of Applied Mechanics, Department of Mechanical Engineering, École Polytechnique, Montréal, Québec, Canada

ARTICLE INFO

Article history:
Accepted 24 April 2017

Keywords:
Spine
Facet
Lumbar ligaments
Intradiscal pressure
Finite element model
Muscles

ABSTRACT

A number of geometrically-detailed passive finite element (FE) models of the lumbar spine have been developed and validated under *in vitro* loading conditions. These models are devoid of muscles and thus cannot be directly used to simulate *in vivo* loading conditions acting on the lumbar joint structures or spinal implants. Gravity loads and muscle forces estimated by a trunk musculoskeletal (MS) model under twelve static activities were applied to a passive FE model of the L4-L5 segment to estimate load sharing among the joint structures (disc, ligaments, and facets) under simulated *in vivo* loading conditions. An equivalent follower (FL), that generates IDP equal to that generated by muscle forces, was computed in each task. Results indicated that under *in vivo* loading conditions, the passive FE model predicted intradiscal pressures (IDPs) that closely matched those measured under the simulated tasks (R^2 = 0.98 and root-mean-squared-error, *RMSE* = 0.18 MPa). The calculated equivalent FL compared well with the resultant force of all muscle forces and gravity loads acting on the L4-L5 segment (R^2 = 0.99 and *RMSE* = 58 N). Therefore, as an alternative approach to represent *in vivo* loading conditions in passive FE model studies, this FL can be estimated by available in-house or commercial MS models. In clinical applications and design of implants, commonly considered *in vitro* loading conditions on the passive FE models do not adequately represent the *in vivo* loading conditions under muscle exertions. Therefore, more realistic *in vivo* loading conditions should instead be used.

1. Introduction

The human spine is subject to varying compressive and shear loads that play a crucial role in the etiology of low back disorders. Proper knowledge of these loads, therefore, is required in the design and development of effective injury prevention, treatment programs and spinal implants. Few attempts have been made to quantify the spinal loads *in vivo* by measurements of the intradiscal pressure (IDP), loads on the instrumented implants, or changes in the body stature via stadiometry (Dreischarf et al., 2016). While the two first approaches are invasive, costly, and limited in terms of available volunteers, the third one requires major assumptions in order to estimate spinal loads. Alternatively, computational biomechanical models have been emerged as viable tools.

A number of models with different degrees of complexity have been developed to predict loads on the spine during static and dynamic activities. These models can be classified into two groups. First, musculoskeletal (MS) models with the objective to calculate trunk muscle forces and joint internal loads by simultaneous consideration of recorded kinematics and equilibrium of joint loads (Arjmand and Shirazi-Adl, 2006a; Arjmand et al., 2009, 2010, 2011, 2012, and Arjmand et al., 2013; Cholewicki and McGill, 1996; Damsgaard et al., 2006; Hajihosseinali et al., 2014; Stokes and Gardner-Morse, 1995). To resolve the joint redundancy an optimization- (Arjmand and Shirazi-Adl, 2006b; Stokes and Gardner-Morse, 2001) or electromyogram (EMG)- (Cholewicki and McGill, 1996; Gagnon et al., 2001) driven approach is often employed (Dreischarf et al., 2016; Arjmand et al., 2009 and Arjmand et al., 2010; Mohammadi et al., 2015). Second, geometrically-detailed passive (devoid of muscles) finite element (FE) models of the lumbar spine with the aim to calculate load sharing among and stresses/strains in the joint structures (discs, facets and ligaments) under *in vitro* loading conditions (Dreischarf et al., 2014). Effect of muscle forces in these passive models is often neglected or simplified by applying a follower load (FL) (Naserkhaki et al., 2016a,b; Rohlmann et al., 2006; Shirazi-Adl and Parnianpour, 2000; Shirazi-Adl, 2006); a load whose line of

* Corresponding author at: Sharif University of Technology, Tehran 11155-9567, Iran.
E-mail address: arjmand@sharif.edu (N. Arjmand).

http://dx.doi.org/10.1016/j.jbiomech.2017.04.026
0021-9290/

action follows the lumbar curvature and passes approximately through the vertebral body or endplate centers.

Performance of the foregoing models to predict internal spinal stresses and loads during *in vivo* activities depends directly on the accuracy in simulating trunk muscle forces that are the primary source of loads on the spine (Arjmand and Shirazi-Adl, 2005). MS models usually consider a detailed musculature but a simplified representation of the complex ligamentous motion segments. These joints are often simulated as pivots with or without rotational springs thus allowing no translational degrees-of-freedom (DOFs). Neglecting translation DOFs can have low to moderate effects, depending on the simulated task, on the predicted spinal loads (Ghezelbash et al., 2015). In more accurate MS models, the intervertebral joints are simulated with nonlinear beam elements (Arjmand and Shirazi-Adl, 2005 and Arjmand and Shirazi-Adl, 2006a; Arjmand et al., 2009 and Arjmand et al., 2010) that although allow for translational DOFs and proper nonlinear behavior of the joints but fail also to provide crucial details on the load sharing between joint structures. Moreover, MS models do not provide any direct estimates of IDP; it needs to be evaluated from the predicted spinal compression, segmental rotation and/or disc cross-sectional area (Ghezelbash et al., 2016).

On the other hand, passive FE models consider a detailed representation of the intervertebral joints in which the disc annulus and nucleus, ligaments, facets, bony structures, and endplates are modeled in much details that allows for the prediction of stresses/strains throughout and load sharing among the joint structures. Devoid of muscles, these models are however not appropriate to directly simulate *in vivo* activities. Nevertheless, these passive models have been used to study *in vivo* maximum voluntary movements in flexion, extension, lateral bending, and axial rotation by applying a constant FL of 1175 N and a moment of 7.5 Nm (Dreischarf et al., 2014). Similarly, submaximal flexion and extension activities have been simulated by a constant FL of 100 N and a moment of 10 Nm (Naserkhaki et al., 2016a). In these studies, it is further assumed that the trunk muscle forces and gravity/inertia loads exert only a compressive FL with no shear force components (Han et al., 2011). Moreover, application of a constant FL cannot accurately simulate the varying compression along the spinal height (Shirazi-Adl and Parnianpour, 2000).

In view of the urgent need to estimate spinal internal stresses and strains under realistic load conditions, the present study hence aims to:

(1) Apply gravity loads and estimated muscle forces from a validated MS trunk model (Arjmand and Shirazi-Adl, 2005, 2006a; Arjmand et al., 2009 and Arjmand et al., 2010) during various static activities as input to drive a geometrically-detailed passive FE model of the L4-L5 motion segment and compute IDP, facet joint forces (FJFs), and ligament forces.
(2) Estimate an equivalent FL that yields IDP equal to that under gravity and muscle force exertions for each task. These equivalent FLs could replace muscle forces whose estimation requires MS modeling.

2. Methods

2.1. MS model

Trunk muscle forces predicted by our previously-validated MS model under twelve static tasks (see below) were used (Arjmand and Shirazi-Adl, 2005 and Arjmand and Shirazi-Adl, 2006a; Arjmand et al., 2006, 2009 and Arjmand et al., 2010). The model consisted of six quadratic shear deformable beams with nonlinear properties to represent T12-S1 segments and seven rigid elements to represent T1-T12 (as a single body) and lumbosacral vertebrae (L1-S1) (Fig. 1a). For a total body weight of 68.4 kg and based on available anthropometric data, an upper body weight of 344.4 N was considered in the model. Weights of upper arms (35.6 N), forearms/hands (29.3 N) and head (46 N) were applied at their mass centers estimated based on *in vivo* measurements. The remaining upper body weight (233.4 N) was distributed eccentrically from the T1 to the L5 (Pearsall, 1994). The weight in hands was applied at its location measured *in vivo*.

A sagittally-symmetric muscle architecture with 56 muscle fascicles was considered (Stokes and Gardner-Morse, 1999) (Fig. 1b and c). Inputs into the model for each simulated task, based on earlier measurements (Arjmand et al., 2009 and Arjmand et al., 2010), were the thorax sagittal rotation (T), pelvis sagittal rotation (P), hand load and distributed gravity loads. Total lumbar rotation ($L = T - P$), was subsequently partitioned between individual thoracolumbar vertebrae (T12 to L5) in accordance with the proportions reported in earlier investigations (Arjmand and Shirazi-Adl, 2006a). To resolve the redundancy at each spinal level, an optimization algorithm with the cost function of sum of cubed muscle stresses was employed.

2.2. Passive FE model

CT-scans at 0.625 mm thickness were taken from a healthy male (35 years old, 75 kg, and 178 cm) to reconstruct 3D geometry of the L4-L5 bony structures (Fig. 2a). The institutional ethic committee's approval and informed consent were obtained. The bony structures and endplates were meshed in ABAQUS (Simulia Inc., Providence, RI) using 4-node tetrahedral solid elements (Fig. 2b). The mesh of two intervening endplates was used to create the disc by extruding eight circumferential composite layers of collagenous fibers embedded in a ground substance (Shirazi-Adl et al., 1984 and 1986; Shirazi-Adl, 2006) and the nucleus cavity (Fig. 2c). The layers were reinforced by rebar elements distributed in concentric lamellae with crosswise pattern at $\sim\pm30^\circ$ (Little, 2004) to represent the annular fibers. Seven spinal ligaments (Fig. 2b) were modeled by axial tension-only connector elements. A frictionless surface to surface contact with a minimum articulation gap distance of 0.6 mm (Dreischarf et al., 2014; Sharma et al., 1998) was used to simulate the facet joints. Material properties of different joint structures are given in Table 1.

2.3. Validations

Validation of the MS model is described elsewhere (Arjmand and Shirazi-Adl, 2006a,b; Arjmand et al., 2009, 2010, 2011 and Arjmand et al., 2012; Rajaee et al., 2015). As for the passive FE model, predicted range of motion (RoM), IDP, and FJFs under a number of *in vitro* loading conditions (single and combined moments and FL) were compared with available *in vitro* and numerical data (see Section 3).

2.4. Matching the passive FE with MS model

The passive FE model that predicts detailed load-sharing should have geometry and passive properties similar to those in the MS model. To do this, the initial L4 and L5 inclinations were taken identical by rigidly rotating the initial passive FE model (constructed from CT images in the supine posture) by 2.5° posterior-wise. This resulted in the orientation of the L4 and L5 mid-planes at respectively 88° and 80° (to the horizontal plane) and thus a local L4-L5 lordosis of 8° (Fig. 3). In addition, nonlinear gross moment-rotation responses were similar in both models (see Section 3) as nonlinear passive properties of both models were mainly set based on identical works (Shirazi-Adl, 2006; Shirazi-Adl et al., 1984 and 1986). Disc cross-sectional area and mid-disc height in the passive FE model (1200 mm^2 and 11 mm) were smaller than those in the MS model (1455 mm^2 and 13.2 mm) by ~17%.

2.5. Simulated tasks

A total of twelve *in vivo* symmetric and asymmetric static activities in upright and flexed postures (Fig. 4) were considered from earlier MS model studies (Arjmand et al., 2009 and Arjmand et al., 2010; Ghezelbash et al., 2016). These tasks were chosen because the corresponding measured L4-L5 IDP (Wilke et al., 2001) as well as the required kinematics (Arjmand et al., 2009 and Arjmand et al., 2010) to drive simulations were already available. The muscle forces estimated by the MS model (based on the equilibrium of moments at all levels and optimization) were subsequently prescribed into the passive FE model along with all upper gravity loads as well as task-specific kinematics (rotations) of the L4 and L5 vertebrae. To do so, the L4 and L5 vertebral bodies were first rigidly rotated about their centroids in the passive FE model to match those in the MS model for the *in vivo* task under consideration (identical orientations in the MS and passive FE model). Subsequently, vector sum of all gravity loads (i.e., weight of the upper trunk plus load in hands in case of lifting tasks) and force in muscles with upper insertions at and above the L4 vertebra were calculated from the MS model (based on the equilibrium of forces at the L4 center). These resultant forces were then applied to the center of L4 vertebral body in the passive FE model. Finally, model responses including L4-L5 IDP, ligament forces and FJFs were computed under prescribed rotations and resultant forces. For the sake of validation in each simulated task, the predicted L4-L5 IDP by the passive FE model was compared with the corresponding *in vivo* measured IDP (Wilke et al., 2001). Moreover, L4-L5 IDP was inde-

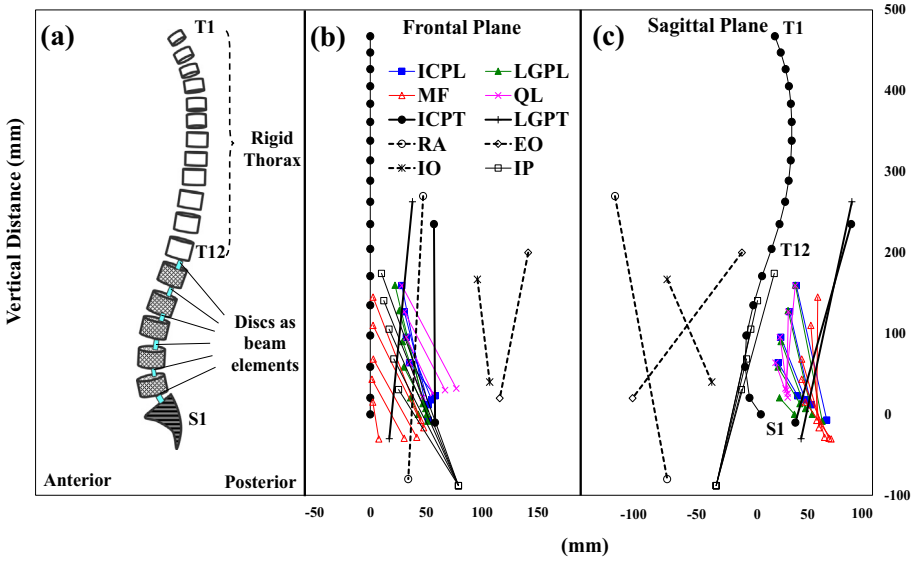

Fig. 1. A schematic of (a) the musculoskeletal model (MS model) as well as its musculatures in (b) the frontal and (c) sagittal planes (only fascicles on one side are shown). ICPL: iliocostalis, lumborum pars lumborum, ICPT, iliocostalis lumborum pars thoracic; IP, iliopsoas; LGPL, longissimus thoracis pars lumborum; LGPT, longissimus thoracis pars thoracic; MF, multifidus; QL, quadratus lumborum; IO, internal oblique; EO, external oblique; RA, rectus abdominus. To simulate curved paths of back muscles in forward flexion tasks, wrapping of global extensor muscles around lumbar vertebrae along with generated contact forces were considered (Arjmand et al., 2006). The deformable beams represented the overall nonlinear stiffness of T12-S1 motion segments (i.e., vertebrae, discs, facets and ligaments) (Arjmand and Shirazi-Adl, 2006a; Shirazi-Adl, 2006).

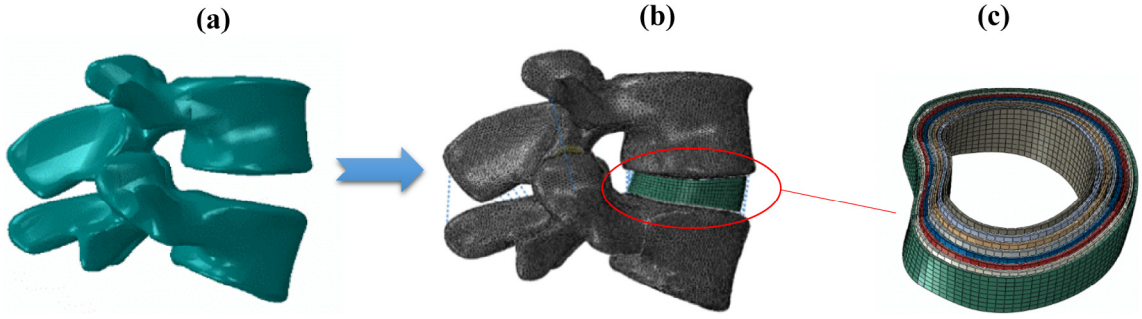

Fig. 2. The passive FE model of the L4-L5 motion segment: (a) 3D reconstruction of the bony elements, (b) mesh generation, and (c) eight circumferential layers of disc annulus. Anterior longitudinal ligament (ALL), posterior longitudinal ligament (PLL), capsular ligament (CL), intertransverse ligament (ITL), ligamentum flavium (LF), supraspinous ligament (SSL), and interspinous ligament (ISL) were considered in the model.

pendently estimated in the MS model based on the associated axial compression force and intersegmental flexion rotation using a quadratic regression equation (Ghezelbash et al., 2016).

Each *in vivo* task was also analyzed in the passive FE model under the same kinematics with an equivalent compressive FL (replacing all gravity and muscle forces). This equivalent FL was determined by trial-and-error so as to yield an IDP identical to that predicted by the FE model under muscle exertions and gravity loads. The FL was applied using pre-compressed unidirectional springs inserted between the centroids of the L4 and L5 vertebral bodies (Naserkhaki et al., 2016a). For simulations of the *in vivo* tasks, the translational degrees of freedom of the lower endplate and facet joints of the L5 vertebra were kept always fixed while translational degrees of freedom of the L4 vertebrae were free.

3. Results

3.1. Validation of the passive FE model

Under pure moment of 10 Nm in different planes, the passive FE model yielded results in overall agreement with the data of the literature as well as the MS model (e.g., root-mean-squared-error, *RMSE*, between predictions of the MS and passive FE model were smaller than 0.25° in the sagittal plane) (Fig. 5a). Under pure FL up to 1000 N, the model predicted IDPs within the *in vitro* range (Rohlmann et al., 2001) as well as other FE model data (Dreischarf et al., 2014; Naserkhaki et al., 2016a) (Fig. 5b). Under 7.5 Nm moments in different anatomical planes along with a FL of 1175 N, the model also predicted IDPs (Fig. 6a), RoMs (Fig. 6b), and FJFs (Fig. 6c) within the range of computed and measured data.

3.2. Predictions for in vivo tasks

The vertical forces (due to muscles and gravity) and horizontal forces (due to muscles) on the L4-L5 motion segments were taken from the MS model (Table 2) and applied into the passive FE model that in turn computed IDP, FJFs, and ligament forces. Moreover, for each *in vivo* activity, the kinematics of the motion segment in the MS model (Table 2), i.e., L4 and L5 rotations with respect to the initial configuration in the supine posture, were also obtained from the MS model (Table 2) and prescribed into the FE model. The passive FE model predicted IDPs (under muscle forces and gravity loads) in overall agreement with the corresponding *in vivo* measured data (R^2 = 0.98 and *RMSE* = 0.18 MPa). The estimated IDPs directly from the MS model were also in overall agreement with the measured IDPs (R^2 = 0.98 and *RMSE* = 0.21 MPa) (Fig. 7). Compared to the upright standing posture with no load, forces in posterior ligaments increased with the trunk forward flexion angle but

Table 1
Material properties of different structures in the passive FE model of the L4-L5 motion segment. Cortical and cancellous bones were assigned transversely isotropic linear elastic material properties while bony endplates, cartilaginous endplates and posterior bony elements were taken as linear elastic isotropic materials. The annulus ground substance was modeled as a Mooney-Rivlin hyper-elastic material and nucleus as an incompressible fluid-filled cavity. Nonlinear force-displacement curves were used for ligaments. The annular fibers (rebars) had nonlinear force-displacement relationship with stiffness increasing from inner to outer lamellae.

Structure	Modulus of elasticity (MPa)	Poisson's ratio	Reference
Cortical bone	E_{xx} = 11300 E_{yy} = 11300 E_{zz} = 22000 G_{xy} = 3800 G_{yz} = 5400 G_{xz} = 5400	ν_{xy} = 0.484 ν_{yz} = 0.203 ν_{xz} = 0.203	Lu et al. (1996)
Cancellous bone	E_{xx} = 140 E_{yy} = 140 E_{zz} = 200 G_{xy} = 48.3 G_{yz} = 48.3 G_{xz} = 48.3	ν_{xy} = 0.45 ν_{yz} = 0.315 ν_{xz} = 0.315	Lu et al. (1996)
Cartilaginous endplate	E = 23.8	ν = 0.4	Lu et al. (1996)
Bony endplate	E = 12000	ν = 0.3	Edwards et al. (2001)
Posterior bony structure	E = 3500	ν = 0.25	Shirazi-Adl et al. (1986)
Annulus ground substance	Mooney-Rivlin (C_{10} = 0.18, C_{01} = 0.045)		Schmidt et al. (2007)
Annulus fibers	Nonlinear stress-strain curves		Shirazi-Adl et al. (1984) and (1986)
Nucleus pulposus	Incompressible fluid-filled cavity		Park et al. (2013) and Shirazi-Adl, 1992
Ligaments	Nonlinear force-displacement curves		Shirazi-Adl et al. (1986)

decreased in symmetric and asymmetric loaded tasks with 19.8 kg in hands (Table 2). FJFs were small in the symmetric neutral upright and flexed postures with no loads in hands but considerably increased in asymmetric tasks and when a 19.8 kg load was held in hands (Table 2). The equivalent FL, that generates IDP identical to that by muscle forces for each task, was found to increase considerably with trunk rotations and remain close to the resultant force of muscle forces and gravity loads (R^2 = 0.99 and *RMSE* = 58 N) (Table 2). Moreover, the equivalent FL not only generated IDP identical to that by muscle forces for each task but resulted in the similar ligament forces (*RMSE* < 1 N) and FJFs (*RMSE* < 2 N) as those predicted under muscle forces (Table 3).

4. Discussion

While trunk MS models fail to predict the *in vivo* load sharing between different spine joint structures, passive FE models, by not incorporating active musculature, remain inappropriate for simulation of *in vivo* tasks. A coupled hybrid model representing both musculature and detailed passive structures would circumvent these shortcomings. This study proposed an uncoupled solution to this problem in which the applied kinematics and estimated muscle forces in a MS model of an *in vivo* task were used to drive a passive FE model that predicted stresses/strains in various components. With this approach, the predicted L4-L5 IDPs for a number of *in vivo* activities matched measured IDPs (Fig. 7). Such staggered solution can hence be used to simulate *in vivo* activities if appropriate kinematics (from imaging or skin motion analysis) and *in vivo* loading conditions under muscle exertions (from a detailed MS model) are considered into the passive model. Alternatively, an equivalent FL (specific to each task) can replace muscle and gravity loads. In clinical applications or design and development of implants, the passive FE models should be used under *in vivo* loading conditions obtained from MS models rather than *in vitro* loading conditions (i.e., pure moments with or without a FL).

4.1. Limitations

Limitations of the MS model have been discussed elsewhere (Arjmand and Shirazi-Adl, 2006a). In brief, the optimization-driven MS model fails to predict any antagonistic muscle forces.

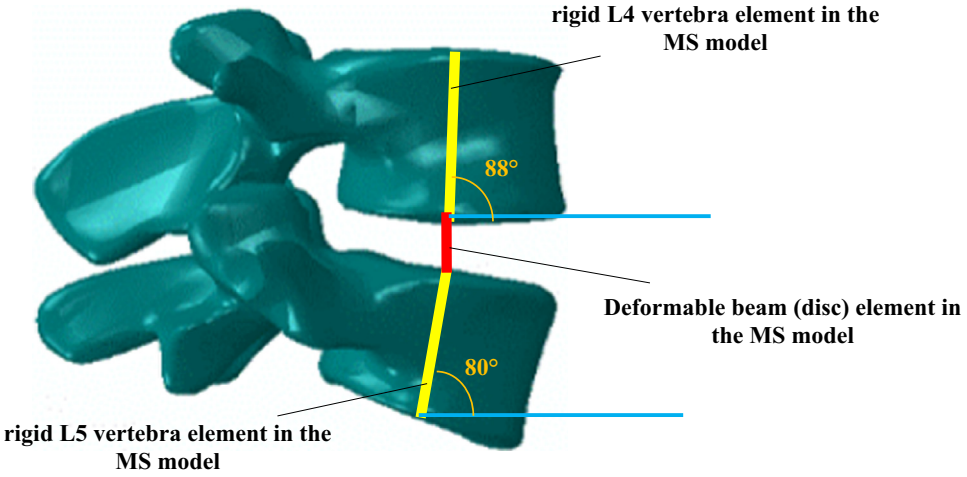

Fig. 3. A schematic of the matched FE and MS models in terms of their angular kinematics.

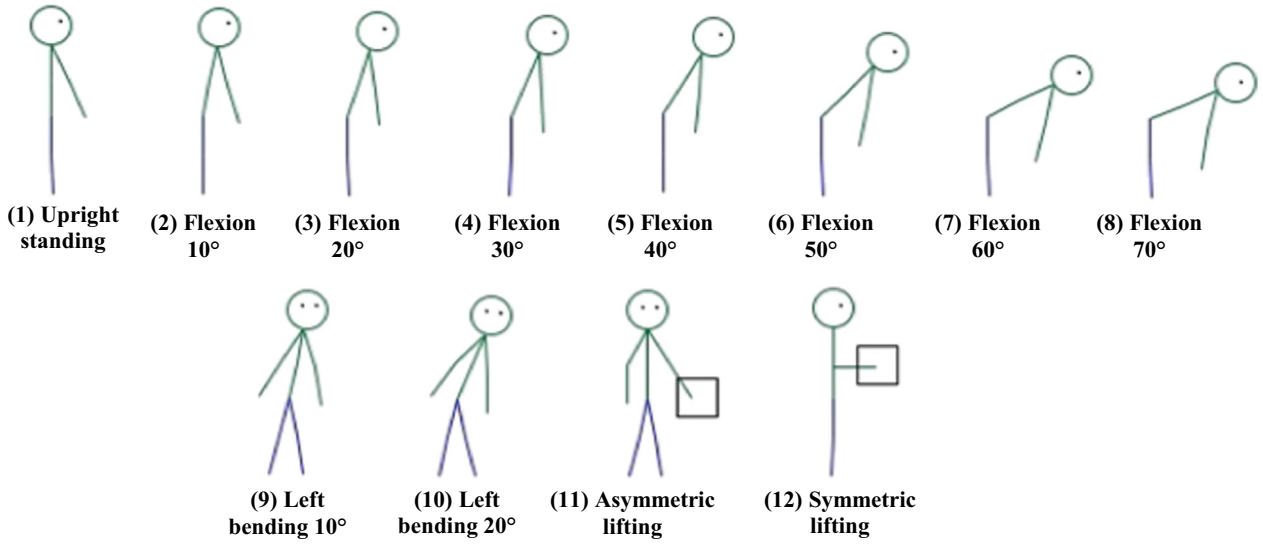

Fig. 4. Schematics of the twelve tasks simulated by the MS model to predict muscle forces and by the passive FE model to predict joint loads. (1) neutral upright standing posture with no load in hands located at ~15 cm anterior to the L5-S1 disc, (2–8) symmetric forward upper trunk flexion by 10, 20, 30, 40, 50, 60, and 70° (total trunk inclination with respect to the upright posture) without hand load (arms freely hanging in the gravity direction), (9) left lateral bending of the upper trunk by 10° (arms kept on the sides), (10) left lateral bending of the upper trunk by 20° (arms hanging on sides), (11) asymmetric one-handed lift of 19.8 kg on the left side at ~34 cm lateral and 0 cm posterior to the L5-S1 disc in the upright posture, and (12) symmetric two-handed lift of 19.8 kg at 25 cm anterior distance to the L5-S1 disc in the upright posture.

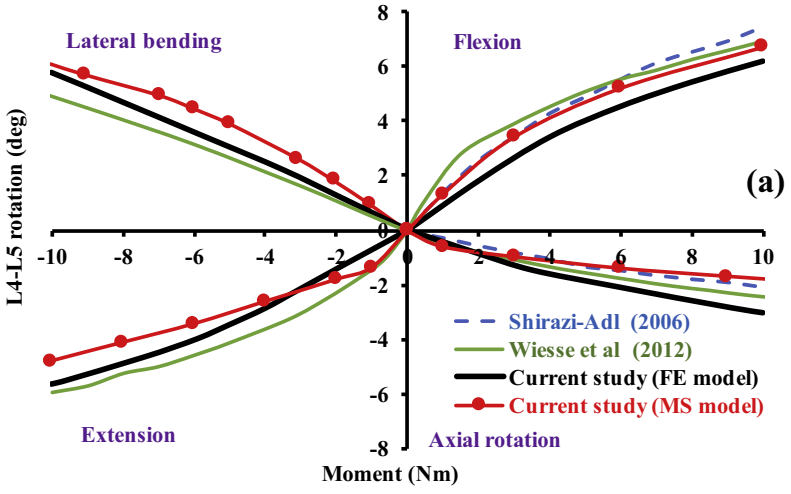

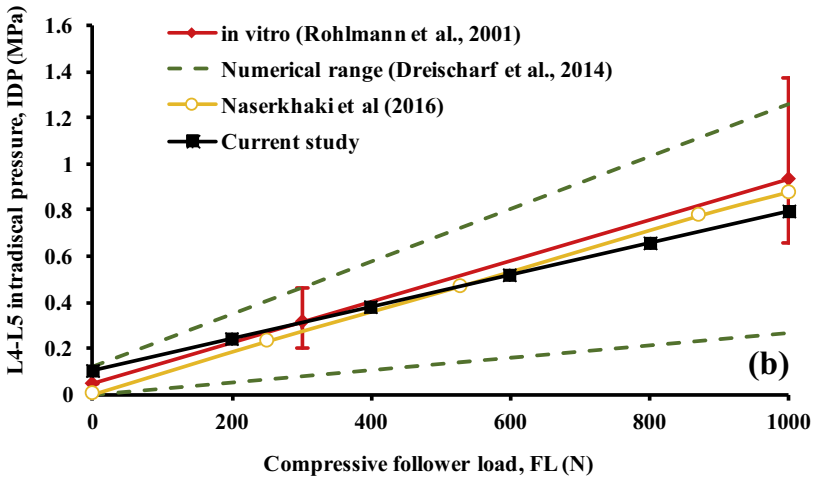

Fig. 5. Comparison between predictions of the passive FE model and the exiting experimental and numerical data obtained under *in vitro* loading conditions: (a) pure moment of up to 10 Nm and (b) pure follower load (FL) of up to 1000 N. Data of Dreischarf et al. (2014) are based on eight different FE models available in the literature.

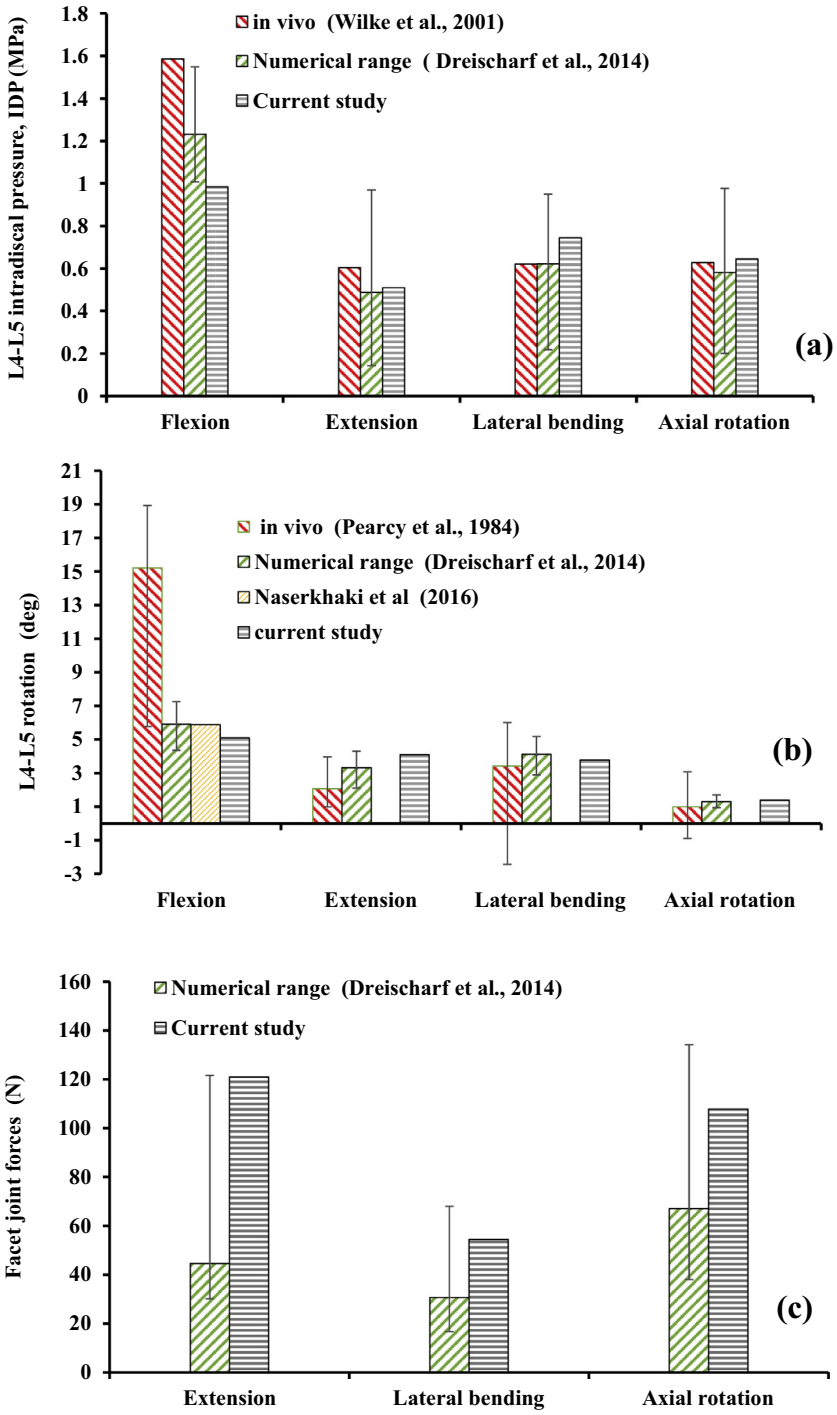

Fig. 6. Comparison between predictions of the passive FE model and the exiting experimental and numerical data obtained under *in vitro* loading conditions (7.5 Nm of moment and 1175 N of follower load): (a) L4-L5 intradiscal pressure (IDP), (b) L4-L5 range of motion (RoM), and (c) total L4-L5 facet joint forces. Numerical range refers to the range of data predicted by eight validated finite element models (Dreischarf et al., 2014). This loading condition (7.5 Nm of moment and 1175 N of follower load) does not necessarily represent *in vivo* loading situations (as these should be simulated under muscle forces) but similar to other modeling studies such comparisons with *in vivo* data were nevertheless made. This may explain the discrepancy between the model predictions and data measured under *in vivo* conditions (e.g., L4-L5 IDP and RoM in flexion).

Despite a detailed muscle architecture (Fig. 1), intersegmental muscles as well as transverse abdominis muscle and its effect on the intra-abdominal pressure were neglected. The thoracic spine was considered to be rigid; an assumption that slightly affects the lower lumbar spine loads (Ignasiak et al., 2016). As for the passive FE model, while a wide range of material properties are reported in the literature for nonlinear behavior of the annulus ground substance, annulus fibers, and ligaments we intentionally considered those reported by Shirazi-Adl et al. (1984 and 1986). This was because passive properties of the intervertebral discs (beams) in the MS model were also based on the same works. Comparison between moment-rotation behaviors of the passive FE model with those of the MS model indicated close agreement (Fig. 5a) as intended. The passive FE model included only one single level (L4-L5); we could not therefore predict IDP, FJFs, and ligament forces at other lumbar levels for the simulated *in vivo* activities.

Table 2
Outputs of the MS model for the *in vivo* loading condition of each simulated task as well as outputs of the passive FE model for ligament and facet joint forces (FJFs). The equivalent follower load (FL) whose application in the passive FE model results in the same intradiscal pressures (IDP) as those obtained by application of muscle forces is also presented. All rotations (degrees) are positive for anterior direction in the sagittal plane and for left direction in the frontal plane (rotations are given relative to the supine posture in which geometry of the passive FE model is built). All forces are in N. Vertical forces are positive downward, horizontal forces are positive anterior, and lateral forces are positive toward left. For the asymmetric tasks, the posture remains symmetric similar to those in the upright standing posture.

	MS model outputs = Passive FE model inputs						Passive FE model outputs									
Symmetric tasks	Sagittal L4 rotation	Sagittal L5 rotation	Vertical force (N)	Horizontal force (N)	Resultant force (N)	L4-L5 lordosis	Ligament forces (N)							FJF (N)		Equivalent
							ALL	PLL	ITL	ISL	SSL	CL	LF	Left	Right	FL (N)
Upright standing	−6.8	−8.4	440.0	15.0	440.3	6.4	0.0	0.7	2.5	5.9	0.2	0.0	0.0	2.5	2.0	451.0
Flexion 10°	−1.1	−4.3	672.1	−9.7	672.2	4.8	0.0	1.5	1.0	5.6	1.1	0.6	3.5	0.0	0.0	692.6
Flexion 20°	5.4	1.0	963.8	−117.2	970.9	3.6	0.0	2.3	1.1	5.9	1.2	6.4	5.6	0.0	0.0	981.0
Flexion 30°	11.1	5.1	1189.7	−277.8	1221.7	2.0	0.0	4.9	1.8	6.6	1.3	12.1	6.1	0.0	0.0	1225.8
Flexion 40°	16.9	9.4	1362.7	−481.0	1445.1	0.5	0.0	8.3	3.8	7.8	4.7	37.1	7.3	0.0	0.0	1454.4
Flexion 50°	22.3	13.0	1447.1	−681.4	1599.5	−1.3	0.0	12.0	8.2	9.2	12.1	82.5	9.2	0.0	0.0	1593.8
Flexion 60°	27.9	16.9	1472.4	−888.4	1719.7	−3.0	0.0	18.7	14.1	22.9	24.3	146.7	10.5	0.0	0.0	1709.7
Flexion 70°	35.2	23.3	1443.3	−1146.5	1843.3	−3.9	0.0	25.0	21.2	38.6	39.4	210.2	11.1	0.0	0.0	1762.4
Symmetric lifting	−9.3	−5.3	1366.4	261.5	1391.2	12.0	24.9	0.0	0.0	0.0	0.0	23.3	0.0	182.7	172.3	1553.2
Asymmetric tasks	Lateral L4 rotation	Lateral L5 rotation	Vertical force (N)	Horizontal force (N)	Lateral force (N)	Resultant force (N)	Ligament forces (N)							FJF (N)		Equivalent
							ALL	PLL	ITL	ISL	SSL	CL	LF	Left	Right	FL (N)
Lateral bending 10°	4.4	2.1	574.1	37.8	31.0	576.2	0.0	0.1	2.6	4.0	1.1	0.5	1.4	13.1	5.9	580.7
Lateral bending 20°	8.9	4.3	721.8	53.1	83.7	728.6	0.0	0.2	4.2	4.2	1.3	1.8	1.6	45.2	29.8	750.5
Asymmetric lifting	−6.8	−8.4	1560.0	22.6	0.4	1560.2	0.0	0.0	0.0	0.0	0.1	0.0	0.0	25.3	23.1	1637.8

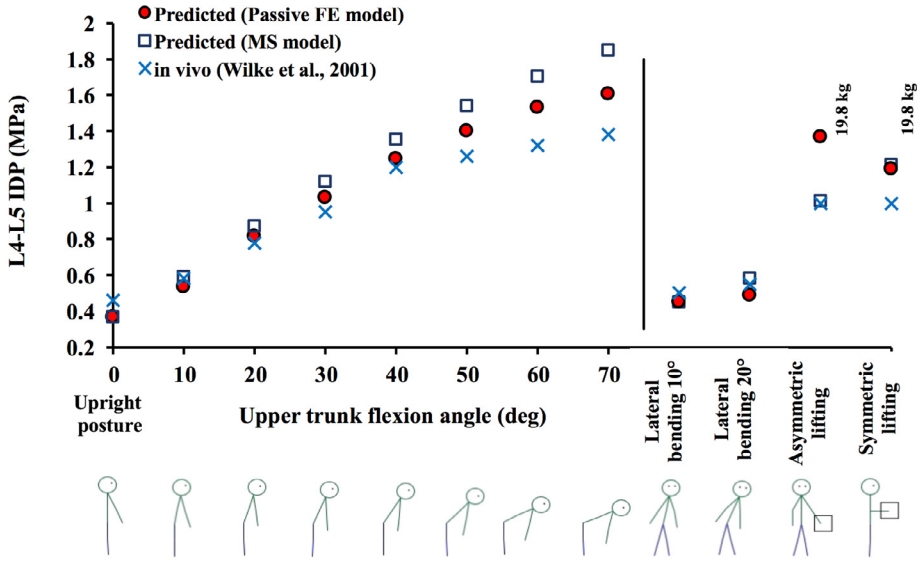

Fig. 7. L4-L5 intradiscal pressure (IDP) predicted by the passive FE model under muscle forces and L4-L5 IDP estimated directly from the MS model as compared with the measured *in vivo* data under similar tasks. *In vivo* values for flexion angles of 50, 60, and 70° were estimated using interpolation from data provided by Wilke et al. (2001).

Table 3
The equivalent compressive follower loads (FL) for each task that yields intradiscal pressure (IDP) equal to that predicted under gravity and muscle force exertions. The associated ligament forces and facet joint forces (FJFs) under the equivalent FL are also reported.

Symmetric tasks	Equivalent	Ligament forces (N)							FJF (N)	
	FL (N)	ALL	PLL	ITL	ISL	SSL	CL	LF	Left	Right
Upright standing	451.0	0.0	0.7	2.3	5.5	0.2	0.0	0.0	2.3	1.7
Flexion 10°	692.6	0.0	1.4	1.0	5.3	1.0	0.5	3.2	0.0	0.0
Flexion 20°	981.0	0.0	2.3	1.1	5.6	1.0	6.3	5.5	0.0	0.0
Flexion 30°	1225.8	0.0	4.6	1.7	6.5	1.2	11.9	6.1	0.0	0.0
Flexion 40°	1454.4	0.0	7.9	3.8	7.6	3.5	37.0	7.0	0.0	0.0
Flexion 50°	1593.8	0.0	12.0	8.2	9.2	10.9	81.2	9.1	0.0	0.0
Flexion 60°	1709.7	0.0	18.5	14.0	22.0	23.0	142.0	10.4	0.0	0.0
Flexion 70°	1762.4	0.0	25.0	21.0	37.9	38.5	204.9	10.8	0.0	0.0
Symmetric lifting	1553.2	23.7	0.0	0.0	0.0	0.0	21.9	0.0	185.4	175.3
Asymmetric tasks	Equivalent	Ligament forces (N)							FJF (N)	
	FL (N)	ALL	PLL	ITL	ISL	SSL	CL	LF	Left	Right
Lateral bending 10°	580.7	0.0	0.1	2.4	3.7	1.0	0.4	1.1	12.5	5.0
Lateral bending 20°	750.5	0.0	0.2	3.9	4.0	1.3	1.5	1.5	40.9	26.7
Asymmetric lifting	1637.8	0.0	0.0	0.0	0.0	0.0	0.0	0.0	22.6	20.8

4.2. Validation

Predictions of the passive FE model under *in vitro* loading conditions including pure moment (Fig. 5a), pure FL (Fig. 5b), and a combination thereof (Fig. 6) were within the range of measured *in vitro* (Rohlmann et al., 2001) and computed (Dreischarf et al., 2014; Naserkhaki et al., 2016a) data. Due to the paucity of *in vivo* measurements, we only compared our predictions for the L4-L5 IDP with those recorded in one subject (Wilke et al., 2001) (Fig. 7). The body weight and height (68.4 kg and 174.5 cm) considered in the MS model were close to those of the male subject (70 kg and 168 cm) that participated in the IDP measurements (Wilke et al., 2001). This concordance makes such comparison more relevant as our recent investigations indicate that body weight markedly influences spinal loads (Ghezelbash et al., 2016; Hajihosseinali et al., 2015). Such comparisons remain however qualitative as disc cross-sectional areas were quite different; 1800 mm^2 in the single subject (Wilke et al., 2001) versus 1200 mm^2 and 1455 mm^2 in our passive FE and MS models, respectively. Disc geometrical parameters (height and area) also affect model predictions (Dreischarf et al., 2014; Natarajan and Andersson, 1999; Zander et al., 2017). Moreover, *in vivo* IDP were collected in only one subject thus neglecting the inter-individual variabilities. These, along with the abovementioned simplifications made in the MS model to estimate muscle forces, may explain the discrepancy between IDP measured *in vivo* and predicted by the FE and MS especially at larger flexion angles. Moreover, the regression equation used to estimate the L4-L5 IDP in the MS model (Ghezelbash et al., 2016) is only suitable for sagittally symmetric tasks involving flexion intersegmental rotations that may affect the estimated IDP for the asymmetric lifting task (Fig. 7).

FJFs vanished in tasks involving forward trunk flexion and increased in the symmetric lifting (19.8 kg) task (Table 2). To hold the load in front in the symmetric lifting tasks (Fig. 4), the upper trunk and thus L4-L5 motion segment extended backward (by 4°) (Table 2) that along with the increased compressive load (due to the hand load) resulted in a considerable increase in the FJFs. Similar trends have been reported in earlier single motion segment studies under compression force with or without sagittal rotations (Shirazi-Adl and Drouin, 1987). Forces in posterior and anterior ligaments, as expected, increased in tasks with greater segmental rotations in flexion and extension, respectively, but decreased in tasks under larger axial compression force (due to smaller tensile strains in the ligaments). Quite distinct ligament force-displacement curves have been suggested in literature (Zander et al., 2004) with the ones considered in the present study falling among the least stiff ones. It has been shown that under a flexion moment of 7.5 Nm at the L3-L4 motion segment, predicted force (by an identical model) in the PLL could vary from ~25 N to 205 N depending on the force-displacement curve considered for this ligament (Zander et al., 2004). A recent modeling investigation, in agreement with our finding, reported that under *in vitro* loading conditions in flexion the maximal force, among all ligaments, is generated in CL (Naserkhaki et al., 2016a).

4.3. Load sharing between different structures

Estimation of load partitioning as well as tissue level stresses and strains under *in vivo* loads allows for a more accurate evaluation of risk of injury when compared to failure threshold of various. For instance, while risk of injury to the disc and facets increased in loaded (more demanding) activities (compare higher IDP and facet forces in symmetric/asymmetric lifting tasks with those in the neutral standing posture), risk of injury to the posterior ligaments reduced in loaded tasks (compare smaller ligament forces in symmetric/asymmetric lifting tasks with those in the neutral standing posture) (Table 2 and Fig. 7). Moreover, while risk of injury to the posterior ligaments and discs increased with the trunk flexion angle, facets were relieved in these tasks.

4.4. Equivalent FL

A single equivalent FL at a magnitude close to the resultant force of gravity loads and muscle forces can be applied to the passive FE model (as an alternative to the gravity loads and muscle force components) to represent the *in vivo* loading condition. This FL was initially estimated in this study by trial-and-error (or by considering the linear relationship between IDP and FL as shown in Fig. 5b) so to yield a L4-L5 IDP identical to that predicted under gravity and muscle exertions. As the L4-L5 rotations under the equivalent FL and muscle forces were identical, ligament and facet forces were also found, as expected, similar under muscle forces and the equivalent FL (Table 3). If a detailed MS model is not available to estimate muscle forces, it is suggested that simplistic single-muscle (e.g., Merryweather et al., 2009; Potvin, 1997), commercial MS models (e.g., University of Michigan Center for Ergonomics, 2014) or our regression equations (Arjmand et al., 2011 and Arjmand et al., 2012) be used to approximate an equivalent FL (equal to the resultant of the spine compressive and shear loads) for the activity under consideration. Results clearly indicate that considering a constant FL (of 1175 N) (Dreischarf et al., 2014) as the *in vivo* loading condition for various maximal voluntary activities in different anatomical planes or a constant FL (of 100 N) (Naserkhaki et al., 2016a) to simulate different submaximal activities in flexed and extended postures is inaccurate. Moreover, a FL of 1175 N appears to be too small to represent the *in vivo* loading in maximal voluntary flexion as according to our MS and passive FE models this magnitude corresponds to trunk flexion angle of only ~30° (Table 2) and its application to the passive FE model yields IDP in agreement with the measured IDP in this flexion angle (Fig. 7).

In summary, a staggered (uncoupled) detailed passive model-active MS model investigation was performed to predict tissue-level stresses and load partitioning in spinal segments under various *in vivo* postures. These loads can be applied to passive FE models when used in clinical applications and design of implants in which consideration of realistic loading conditions is crucial. Accurate load sharing between various passive structures and thus evaluation of risk of injury requires representation of realistic *in vivo* loading conditions.

Conflict of interest statement

The authors have no conflicts of interest concern.

Acknowledgment

This work was supported by grants from Sharif University of Technology (Tehran, Iran). Assistance of Dr. S. Naserkhaki in interpreting the findings and Mr. D. Zarei-Rahmatabadi in providing technical help with the meshing procedure of the passive finite element model is greatly appreciated.

References

Arjmand, N., Ekrami, O., Shirazi-Adl, A., Plamondon, A., Parnianpour, M., 2013. Relative performances of artificial neural network and regression mapping tools in evaluation of spinal loads and muscle forces during static lifting. J. Biomech. 46, 1454–1462.

Arjmand, N., Gagnon, D., Plamondon, A., Shirazi-Adl, A., Lariviere, C., 2009. Comparison of trunk muscle forces and spinal loads estimated by two biomechanical models. Clin. Biomech. 24, 533–541.

Arjmand, N., Gagnon, D., Plamondon, A., Shirazi-Adl, A., Lariviere, C., 2010. A comparative study of two trunk biomechanical models under symmetric and asymmetric loadings. J. Biomech. 43, 485–491.
Arjmand, N., Plamondon, A., Shirazi-Adl, A., Lariviere, C., Parnianpour, M., 2011. Predictive equations to estimate spinal loads in symmetric lifting tasks. J. Biomech. 44, 84–91.
Arjmand, N., Plamondon, A., Shirazi-Adl, A., Parnianpour, M., Larivière, C., 2012. Predictive equations for lumbar spine loads in load-dependent asymmetric one- and two-handed lifting activities. Clin. Biomech. 27, 537–544.
Arjmand, N., Shirazi-Adl, A., 2005. Biomechanics of changes in lumbar posture in static lifting. Spine 30, 2637–2648.
Arjmand, N., Shirazi-Adl, A., 2006a. Model and in vivo studies on human trunk load partitioning and stability in isometric forward flexions. J. Biomech. 39, 510–521.
Arjmand, N., Shirazi-Adl, A., 2006b. Sensitivity of kinematics-based model predictions to optimization criteria in static lifting tasks. Med. Eng. Phys. 28, 504–514.
Arjmand, N., Shirazi-Adl, A., Bazrgari, B., 2006. Wrapping of trunk thoracic extensor muscles influences muscle forces and spinal loads in lifting tasks. Clin. Biomech. 21, 668–675.
Cholewicki, J., McGill, S.M., 1996. Mechanical stability of the in vivo lumbar spine: implications for injury and chronic low back pain. Clin. Biomech. 11, 1–15.
Damsgaard, M., Rasmussen, J., Christensen, S.T., Surma, E., De Zee, M., 2006. Analysis of musculoskeletal systems in the AnyBody Modeling System. Simul. Model. Pract. Theory 14, 1100–1111.
Dreischarf, M., Shirazi-Adl, A., Arjmand, N., Rohlmann, A., Schmidt, H., 2016. Estimation of loads on human lumbar spine: a review of in vivo and computational model studies. J. Biomech. 49, 833–845.
Dreischarf, M., Zander, T., Shirazi-Adl, A., Puttlitz, C., Adam, C., Chen, C., Goel, V., Kiapour, A., Kim, Y., Labus, K., 2014. Comparison of eight published static finite element models of the intact lumbar spine: predictive power of models improves when combined together. J. Biomech. 47, 1757–1766.
Edwards, W.T., Zheng, Y., Ferrara, L.A., Yuan, H.A., 2001. Structural features and thickness of the vertebral cortex in the thoracolumbar spine. Spine 26, 218–225.
Gagnon, D., Larivière, C., Loisel, P., 2001. Comparative ability of EMG, optimization, and hybrid modelling approaches to predict trunk muscle forces and lumbar spine loading during dynamic sagittal plane lifting. Clin. Biomech. 16, 359–372.
Ghezelbash, F., Arjmand, N., Shirazi-Adl, A., 2015. Effect of intervertebral translational flexibilities on estimations of trunk muscle forces, kinematics, loads, and stability. Computer Methods Biomech. Biomed. Eng. 18, 1760–1767.
Ghezelbash, F., Shirazi-Adl, A., Arjmand, N., El-Ouaaid, Z., Plamondon, A., 2016. Subject-specific biomechanics of trunk: musculoskeletal scaling, internal loads and intradiscal pressure estimation. Biomech. Model Mechanobiol. (in press). http://dx.doi.org/10.1007/s10237-016-0792-3.
Hajihosseinali, M., Arjmand, N., Shirazi-Adl, A., Farahmand, F., Ghiasi, M., 2014. A novel stability and kinematics-driven trunk biomechanical model to estimate muscle and spinal forces. Med. Eng. Phys. 36, 1296–1304.
Hajihosseinali, M., Arjmand, N., Shirazi-Adl, A., 2015. Effect of body weight on spinal loads in various activities: a personalized biomechanical modeling approach. J. Biomech. 48, 276–282.
Han, K.-S., Rohlmann, A., Yang, S.-J., Kim, B.S., Lim, T.-H., 2011. Spinal muscles can create compressive follower loads in the lumbar spine in a neutral standing posture. Med. Eng. Phys. 33, 472–478.
Ignasiak, D., Ferguson, S.J., Arjmand, N., 2016. A rigid thorax assumption affects model loading predictions at the upper but not lower lumbar levels. J. Biomech. 49, 3074–3078.
Little, J.P., 2004. Finite element modelling of anular lesions in the lumbar intervertebral disc.
Lu, M.Y., Hutton, W.C., Gharpuray, V.M., 1996. Can variations in intervertebral disc height affect the mechanical function of the disc? Spine 21, 2208–2216.
Merryweather, A.S., Loertscher, M.C., Bloswick, D.S., 2009. A revised back compressive force estimation model for ergonomic evaluation of lifting tasks. Work 34, 263–272.
Mohammadi, Y., Arjmand, N., Shirazi-Adl, A., 2015. Comparison of trunk muscle forces, spinal loads and stability estimated by one stability-and three EMG-assisted optimization approaches. Med. Eng. Phys. 37, 792–800.
Naserkhaki, S., Jaremko, J.L., Adeeb, S., El-Rich, M., 2016a. On the load-sharing along the ligamentous lumbosacral spine in flexed and extended postures: Finite element study. J. Biomech. 49, 974–982.
Naserkhaki, S., Jaremko, JL., El-Rich, M., 2016b. Effects of inter-individual lumbar spine geometry variation on load-sharing Geometrically personalized Finite Element study. J. Biomech.
Natarajan, R.N., Andersson, G.B., 1999. The influence of lumbar disc height and cross-sectional area on the mechanical response of the disc to physiologic loading. Spine 24, 1873–1881.
Park, W.M., Kim, K., Kim, Y.H., 2013. Effects of degenerated intervertebral discs on intersegmental rotations, intradiscal pressures, and facet joint forces of the whole lumbar spine. Comput. Biol. Med. 43, 1234–1240.
Pearsall, D.J., 1994. Segmental Inertial Properties of the Human Trunk as Determined from Computed Tomography and Magnetic Resonance Imagery. Queen's University.
Potvin, J.R., 1997. Use of NIOSH equation inputs to calculate lumbosacral compression forces. Ergonomics 40 (7), 691–707.
Rajaee, M.A., Arjmand, N., Shirazi-Adl, A., Plamondon, A., Schmidt, H., 2015. Comparative evaluation of six quantitative lifting tools to estimate spine loads during static activities. Appl. Ergon. 48, 22–32.
Rohlmann, A., Bauer, L., Zander, T., Bergmann, G., Wilke, H.J., 2006. Determination of trunk muscle forces for flexion and extension by using a validated finite element model of the lumbar spine and measured in vivo data. J. Biomech. 39, 981–989.
Rohlmann, A., Neller, S., Claes, L., Bergmann, G., Wilke, H.-J., 2001. Influence of a follower load on intradiscal pressure and intersegmental rotation of the lumbar spine. Spine 26, E557–E561.
Schmidt, H., Heuer, F., Drumm, J., Klezl, Z., Claes, L., Wilke, H.-J., 2007. Application of a calibration method provides more realistic results for a finite element model of a lumbar spinal segment. Clin. Biomech. 22, 377–384.
Sharma, M., Langrana, N., Rodriguez, J., 1998. Modeling of facet articulation as a nonlinear moving contact problem: sensitivity study on lumbar facet response. J. Biomech. Eng. 120, 118–125.
Shirazi-Adl, A., 1992. Finite-element simulation of changes in the fluid content of human lumbar discs. Mechanical and clinical implications. Spine 17, 206–212.
Shirazi-Adl, A., 2006. Analysis of large compression loads on lumbar spine in flexion and in torsion using a novel wrapping element. J. Biomech. 39, 267–275.
Shirazi-Adl, A., Ahmed, A.M., Shrivastava, S.C., 1986. Mechanical response of a lumbar motion segment in axial torque alone and combined with compression. Spine 11, 914–927.
Shirazi-Adl, A., Drouin, G., 1987. Load-bearing role of facets in a lumbar segment under sagittal plane loadings. J. Biomech. 20, 601–613.
Shirazi-Adl, A., Parnianpour, M., 2000. Load-bearing and stress analysis of the human spine under a novel wrapping compression loading. Clin. Biomech. 15, 718–725.
Shirazi-Adl, S.A., Shrivastava, S.C., Ahmed, A.M., 1984. Stress analysis of the lumbar disc-body unit in compression a three-dimensional nonlinear finite element study. Spine 9, 120–134.
Stokes, I.A., Gardner-Morse, M., 1995. Lumbar spine maximum efforts and muscle recruitment patterns predicted by a model with multijoint muscles and joints with stiffness. J. Biomech. 28, 173–186.
Stokes, I.A., Gardner-Morse, M., 1999. Quantitative anatomy of the lumbar musculature. J. Biomech. 32, 311–316.
Stokes, I.A., Gardner-Morse, M., 2001. Lumbar spinal muscle activation synergies predicted by multi-criteria cost function. J. Biomech. 34, 733–740.
University of Michigan Center for Ergonomics, 2014. 3D Static Strength Prediction Program User's Manual.
Wilke, H.J., Neef, P., Hinz, B., Seidel, H., Claes, L., 2001. Intradiscal pressure together with anthropometric data–a data set for the validation of models. Clin. Biomech. 16, S111–S126.
Zander, T., Rohlmann, A., Bergmann, G., 2004. Influence of ligament stiffness on the mechanical behavior of a functional spinal unit. J. Biomech. 37, 1107–1111.
Zander, T., Dreischarf, M., Timm, A.-K., Baumann, W.W., Schmidt, H., 2017. Impact of material and morphological parameters on the mechanical response of the lumbar spine – a finite element sensitivity study. J. Biomech. 53, 185–190.